

Direct growth of graphene films without catalyst on flexible glass substrates by PECVD

Rui-Xia Miao(苗瑞霞)†, Chen-He Zhao(赵晨鹤), Shao-Qing Wang(王少青)‡, Wei Ren(任卫), Yong-Feng Li(李永锋), Ti-Kang Shu(束体康), and Ben Yang(杨奔)

Citation: Chin. Phys. B, 2021, 30 (**9**): 098101. DOI: 10.1088/1674-1056/abeeec

Journal homepage: http://cpb.iphy.ac.cn; http://iopscience.iop.org/cpb

What follows is a list of articles you may be interested in

Intercalation of germanium oxide beneath large-area and high-quality epitaxial graphene on Ir(111) substrate

Xueyan Wang(王雪艳), Hui Guo(郭辉), Jianchen Lu(卢建臣), Hongliang Lu(路红亮), Xiao Lin(林晓), Chengmin Shen(申承民), Lihong Bao(鲍丽宏), Shixuan Du(杜世萱), and Hong-Jun Gao(高鸿钧)

Chin. Phys. B, 2021, 30 (**4**): 048102. DOI: 10.1088/1674-1056/abe22c

A review of experimental advances in twisted graphene moirè superlattice

Yanbang Chu(褚衍邦), Le Liu(刘乐), Yalong Yuan(袁亚龙), Cheng Shen(沈成), Rong Yang(杨蓉), Dongxia Shi(时东霞), Wei Yang(杨威), and Guangyu Zhang(张广宇)

Chin. Phys. B, 2020, 29 (**12**): 128104. DOI: 10.1088/1674-1056/abb221

Epitaxial synthesis and electronic properties of monolayer Pd_2Se_3

Peng Fan(范朋), Rui-Zi Zhang(张瑞梓), Jing Qi(戚竞), En Li(李恩), Guo-Jian Qian(钱国健), Hui Chen(陈辉), Dong-Fei Wang(王东飞), Qi Zheng(郑琦), Qin Wang(汪琴), Xiao Lin(林晓), Yu-Yang Zhang(张余洋), Shixuan Du(杜世萱), Hofer W A, Hong-Jun Gao(高鸿钧)

Chin. Phys. B, 2020, 29 (**9**): 098102. DOI: 10.1088/1674-1056/abab80

High sensitive pressure sensors based on multiple coating technique

Rizwan Zahoor, Chang Liu(刘畅), Muhammad Rizwan Anwar, Fu-Yan Lin(林付艳), An-Qi Hu(胡安琪), Xia Guo(郭霞)

Chin. Phys. B, 2020, 29 (**2**): 028102. DOI: 10.1088/1674-1056/ab6721

Epitaxial growth and air-stability of monolayer Cu_2Te

K Qian(钱凯), L Gao(高蕾), H Li(李航), S Zhang(张帅), J H Yan(严佳浩), C Liu(刘晨), J O Wang(王嘉鸥), T Qian(钱天), H Ding(丁洪), Y Y Zhang(张余洋), X Lin(林晓), S X Du(杜世萱), H-J Gao(高鸿钧)

Chin. Phys. B, 2020, 29 (**1**): 018104. DOI: 10.1088/1674-1056/ab5781

Direct growth of graphene films without catalyst on flexible glass substrates by PECVD*

Rui-Xia Miao(苗瑞霞)†, Chen-He Zhao(赵晨鹤), Shao-Qing Wang(王少青)‡, Wei Ren(任卫), Yong-Feng Li(李永锋), Ti-Kang Shu(束体康), and Ben Yang(杨奔)

School of Electronic Engineering, Xi'an University of Posts & Telecommunications, Xi'an 710121, *China*

(Received 2 December 2020; revised manuscript received 2 March 2021; accepted manuscript online 16 March 2021)

A hydrogen-plasma-etching-based plasma-enhanced chemical vapor deposition (PECVD) synthesis route without metal catalyst for preparing the graphene films on flexible glass is developed. The quality of the prepared graphene films is evaluated by scanning electron microscopy, x-ray photoelectron spectroscopy, high-resolution transmission electron microscopy, ultraviolet-visible spectroscopy, and electrochemical measurements. In a radio frequency (RF) power range of 50 W–300 W, the graphene growth rate increases with RF power increasing, while the intensity ratio of D- to G-Raman peak (I_D/I_G) decreases. When the RF power is higher than 300 W, the I_D/I_G rises again. By optimizing experimental parameters of hydrogen plasma etching and RF power, the properties of as-prepared flexible graphene on glass are modulated to be able to achieve the graphene's transparency, good electrical conductivity, and better macroscopic uniformity. Direct growth of graphene film without any metal catalyst on flexible glass can be a promising candidate for applications in flexible transparent optoelectronics.

Keywords: graphene, flexible glass, PECVD, RF power

PACS: 81.05.ue, 81.15.Gh **DOI:** 10.1088/1674-1056/abeeec

1. Introduction

Graphene has excellent physical and chemical properties, such as high electrical conductivity and light transmittance. The methods of preparing two-dimensional (2D) graphene include mechanical exfoliation, liquid-phase chemical exfoliation of graphite,[1–3] epitaxial growth,[4] chemical vapor deposition,[5–7] and oxidation-reduction methods.[8,9] The chemical vapor deposition (CVD) has been widely used to synthesize high-quality and uniform graphene films on transition metals,[10] such as copper,[11,12] nickel,[13,14] cobalt, and Pt.[15] However, the CVD-grown graphene on transition metals must be transferred to some insulating substrates for device preparation and performance characterization, which will inevitably cause contamination or defects like wrinkles and cracks. Therefore, the direct formation of graphene on insulating substrates avoids the transfer process and is expected to further improve the quality of graphene films. Recently, Chugh *et al.*[16] reported the low-temperature growth of graphene at 650 °C on non-catalytic SiO_2 and quartz substrates by using a one-step PECVD process. In 2017, Sun *et al.*[17] reported the direct preparation of graphene films on soda-lime glass substrates by PECVD at low temperature. Later, Mischke *et al.*[18] studied the direct growth of graphene on GaN-based light-emitting diodes (LEDs) by PECVD. Most of these studies focused on rigid insulating substrates. Nonetheless, few reports focused on graphene growth on flexible insulating substrates,[19] which is of great significance for flexible transparent electronics. In 2016, Marchena *et al.* used nickel films on a flexible glass substrate as a catalytic surface to prepare single-layer flexible graphene glass.[20] In 2019, Liu *et al.* adopted copper foam-assisted PECVD to directly prepare graphene on flexible glass and mica.[21] In our work, a simple method is developed to grow graphene films on flexible glass (Corning Willow glass) substrates without metal catalyst. The prepared graphene-on-Willow glass exhibits good electrical and optical properties and has potential applications in transparent flexible electronic devices.

2. Experiment

2.1. Fabrication of graphene films

Graphene films were prepared by a PECVD system (KEJIA Furnace, Zhengzhou, China), which was composed of the following four parts: gas flow control meter, radio frequency (RF) plasma source, heating area, and vacuum system. The schematic diagram and photograph of the experimental setup are shown in Figs. 1(a) and 1(b). A quartz tube with an inner diameter of 100 mm was fixed to a double-zone heating fur-

*Project supported by the National Natural Science Foundation of China (Grant No. 51302215), the Joint Research Funds of Department of Science & Technology of Shaanxi Province and Northwestern Polytechnical University, China (Grant No. 2020GXLH-Z-029), and the Natural Science Basic Research Program of Shaanxi Province, China (Grant Nos. 2018JQ6084 and 2019JQ-860).

†Corresponding author. E-mail: miao9508301@xupt.edu.cn

‡Corresponding author. E-mail: Wsqing1212@163.com

© 2021 Chinese Physical Society and IOP Publishing Ltd

nace. The RF plasma source (13.6 MHz) could continuously output RF power, and the transmitting part of the RF plasma source was composed of coil-type copper material. The 100-μm-thick Willow glass with low surface roughness (< 0.5 nm) and high light transmittance (> 90%) is used as the substrate and ultrasonically cleaned for 15 min successively in acetone, ethanol, and deionized water to remove impurities from the glass surface. The preparation process is shown in Fig. 1(c). The cleaned substrates were loaded into a quartz boat in the center position of the heating region of the PECVD furnace tube. Substrates were firstly heated to the growth temperature (700 °C–800 °C) in a mixture of argon (100 sccm) and hydrogen (15 sccm) gas atmosphere. When the temperature in the furnace stabilized at the growth temperature, the Ar gas flow was adjusted to 200 sccm. Then, the RF plasma was ignited, and methane (CH_4; 1 sccm–3 sccm) and hydrogen (8 sccm) were introduced into the tube for growing the graphene on the Willow glass surface for 10 min–150 min. Finally, the Ar and CH_4 gas flows were switched off, and the H_2 gas flow was adjusted to 15 sccm. Then, the H_2 plasma was ignited by RF power of 50 W–350 W to initiate the annealing process and etch the graphene films. After the reaction, the RF power was turned off, and the system was cooled down to room temperature in an Ar/H_2 gas atmosphere.

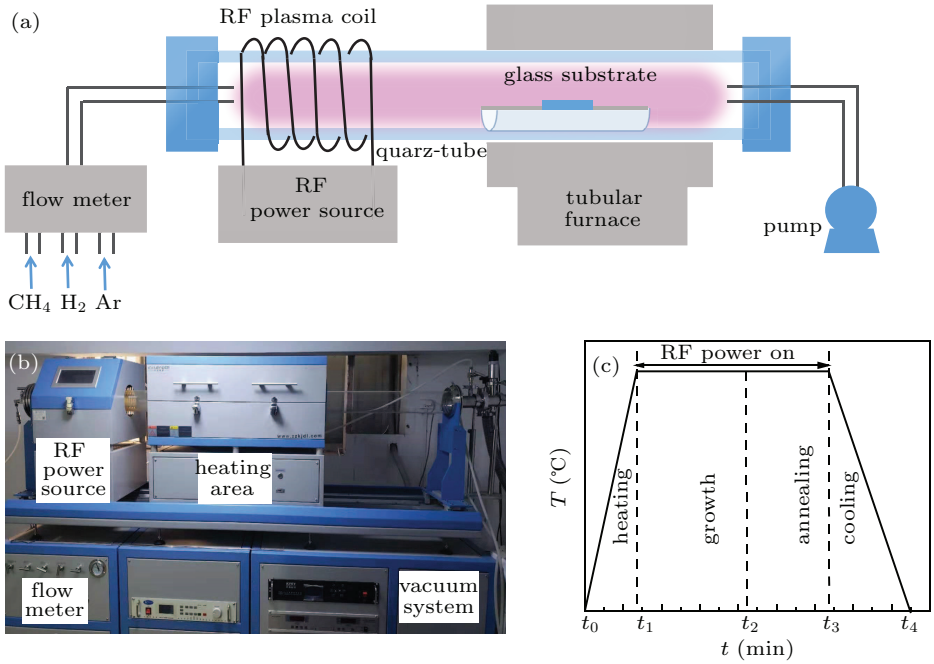


Fig. 1. (a) Schematic diagram and (b) optical image of real setup of the PECVD reactor for graphene growing on Willow glass substrate, and (c) graphene preparation process.

2.2. Material characterizations

The surface morphologies of the graphene films were characterized by scanning electron microscopy (SEM; Sigma-500). The chemical elements and their valence states on the surfaces were analyzed by x-ray photoelectron spectroscopy (XPS; Thermo Fisher 250Xi, USA). Structures and morphologies of the graphene films were analyzed by high-resolution transmission electron microscopy (HR-TEM; JEOL JEM-2100F). Raman spectra were obtained with a 532-nm laser as the excitation light source for frequency shifts in a range from 1000 cm^{-1} to 3000 cm^{-1}. The light transmittance of the film was measured by UV-Vis spectroscopy (Shimadzu UV-2300). *I–V* curves of the thin films were measured by an electrochemical workstation (Shanghai Chenhua, CHI1000C). The electrical properties of the graphene films were determined using a non-contact hall tester (LEI1600).

3. Experimental analysis of growth mechanism

Figure 2 shows the schematic diagram of the graphene growth on flexible Willow glass by PECVD. Willow glass is an amorphous material with completely different chemical bonds and lattice structure from graphene, causing serious lattice mismatch and thermal mismatch between graphene and Willow glass.[22,23] At the initial stage, the impact dissociation of high-energy electrons on methane and a small amount of dehydrogenation reaction decomposes methane into active substances such as CH_x, C_2H_y, and atomic C and H. These active substances are adsorbed on the glass at growth temperatures of 700 °C–800 °C, and a horizontal carbon buffer layer is introduced to release the internal stress between graphene and Willow glass.[24] With increasing growth time, the carbon layers evolve, showing an upward growth trend and extend over the entire Willow glass surface.

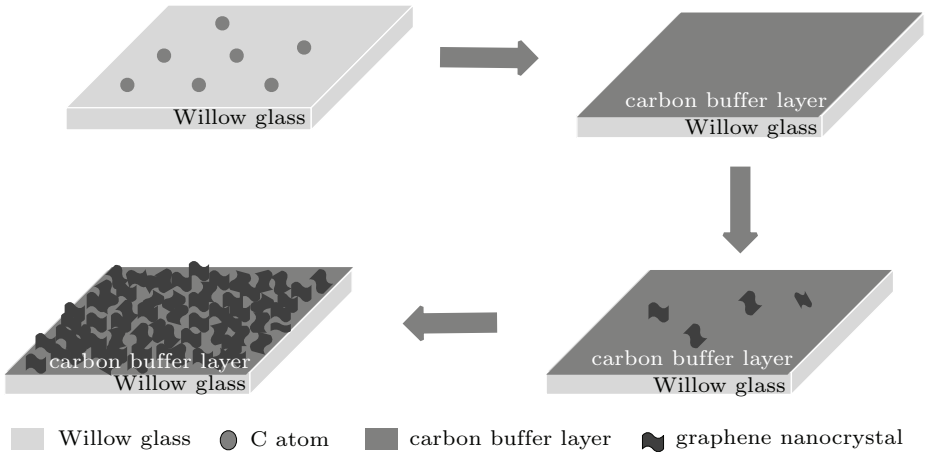


Fig. 2. Schematic diagram of graphene growth on flexible Willow glass.

4. Results and discussion

Previous studies have shown that the surface treatment of graphene films with hydrogen plasma can effectively improve the photoelectric properties.[25,26] Unlike the traditional annealing and hydrogen plasma etching, a new method is used to treat the prepared graphene film: the temperature is kept at a growth temperature of 700 °C–800 °C, and H_2 flow and RF power are set to be 15 sccm and 300 W, respectively. Residual CH_4 in the furnace continues to decompose into CH_x, C_2H_y, and atomic C and H under the etching of H plasma at high temperature.

Methane dehydrogenation with the formation of $(CH_3)^*$ radical ($CH_4 \rightarrow (CH_3)^* + H^*$) should overcome a 1.6-eV ($\sim 16kT$ at 1000 °C) activation barrier, which leads to a rate-limiting step hindering graphene from growing in the absence of additional catalysts such as hydrogen.[27] Hydrogen plasma serves as either an activator of carbon on the substrate or an etching reagent that changes the thickness and defects of graphene on Willow glass.[28] The addition of H_2 results in excited hydrogen atoms (H^*) by the following reaction:

$$H_2 + e^- \rightarrow H^* + H^+. \tag{1}$$

Hydrogen diffusion in plasma is fast so that the H atoms in H plasma can be adsorbed on the walls of the reactor. Subsequently, H atoms in the gaseous phase can combine with the adsorbed H atoms to form vibrationally excited H_2^*. Then, H_2^* can react with hydrogen ions (H^+) according to the following reactions:[29,30]

$$H_2^* + H^+ \rightarrow H_2^+ + H, \tag{2}$$

$$H_2^+ + e^- \rightarrow H + H^*. \tag{3}$$

At that time, a large number of excited H atoms are sufficient for dehydrogenating the methane through reactions (4) and (5). The dissociation mechanism of methane is dominated by the impact of energetic electrons ("physical reaction") and the dehydrogenation effect of hydrogen ("chemical reaction"). Moreover, hydrogen plasma can etch the defects and amorphous carbon produced during the growth of graphene according to reaction (6)[31]

$$CH_x + H^* \rightarrow CH_{x-1} + H_2, \tag{4}$$

$$CH_{x-1} + \text{graphene} \rightarrow (\text{graphene} + C) + H_2, \tag{5}$$

$$H^* + \text{graphene} \rightarrow (\text{graphene} - C) + (CH_x)^*. \tag{6}$$

The Raman spectra of graphene-on-Willow glass before and after etching by hydrogen plasma are shown in Fig. 3(a). The Raman signal of graphene without etching exhibits a small 2D peak and broad peaks, suggesting a low completeness and crystallization degree.[32] After being etched by H plasma, the samples exhibit three distinct Raman peaks at around 1350 cm^{-1} (D peak), 1580 cm^{-1} (G peak), and 2700 cm^{-1} (2D peak), respectively. The sharper G peak implies a better crystallization of graphene after H plasma etching. The *I–V* (current–potential) curves of the samples are shown in Fig. 3(b). The *I–V* slope of the sample before being etched is smaller than that after having been etched by H plasma. The above results clearly show that the graphene films etched by H plasma are beneficial to the improvement of the quality and electrical properties of the samples.

In order to obtain flexible graphene-on-glass samples with better quality, it is necessary to optimize the processing factors of graphene. The key factors include RF power, gas flow rate, growth time, and growth temperature. The quality of the sample is analyzed mainly by Raman spectroscopy. The Raman spectra of graphene/Willow glass samples prepared under different methane gas flow rates are shown in Fig. 4. The growth temperature is fixed at 750 °C for 100 min, and the H_2/Ar ratio is 8/200 sccm. Figure 4(a) shows clear D band, G band, and 2D band peaks of the graphene/Willow glass samples. The relationships between I_D/I_G (black curve, the ratio

between the intensities of D and G peaks) and grain size L_a (blue curve) of samples prepared at different methane gas flow rates are shown in Fig. 4(b). In addition, the grain size L_a of the graphene/Willow glass is calculated from the Tuinstra–Koeing relation[33]

$$L_a = C(\lambda)\left(\frac{I_D}{I_G}\right)^{-1}, \tag{7}$$

where $C(\lambda = 532\ \text{nm}) = \left(2.4 \times 10^{-10}\right)\lambda^4 = 16.03$ nm, and the grain size L_a has a negative correlation with the defect intensity ratio I_D/I_G. When the methane gas flow increases from 1.0 sccm to 2.0 sccm, the density of the carbon source increases, and the intensity ratio of D- to G-Raman peak (I_D/I_G) decreases. However, when the methane gas flow is higher than 2.5 sccm, the I_D/I_G rises again. The grain size L_a has a negative correlation with the defect intensity ratio I_D/I_G. Figure 4(c) shows the variation of I_{2D}/I_G with methane gas flow rate. The I_{2D}/I_G that is the ratio between the intensities of 2D peak and G peak reaches a highest value when the methane gas flow is 2.0 sccm.

Figure 5 shows the Raman spectra of graphene/Willow glass samples prepared at different growth times in a range from 30 min to 150 min. The growth temperature is fixed at 750 °C for 300 W with $CH_4/H_2/Ar$ gas flow rates of 2.0/8.0/200.0 sccm, respectively. When the growth time is less than 30 min, no Raman peak is observed. The I_D/I_G ratio decreases with the increase of the growth time from 30 min to 100 min. Figure 5(c) shows the variation of the I_{2D}/I_G ratio with growth time. The I_{2D}/I_G ratio is around 0.5–0.8, which indicates that the graphene nanowall probably consists of multiple layers. Based on the Raman data of these samples, the growth time is set to be the optimized value of 100 min in the following experiments.

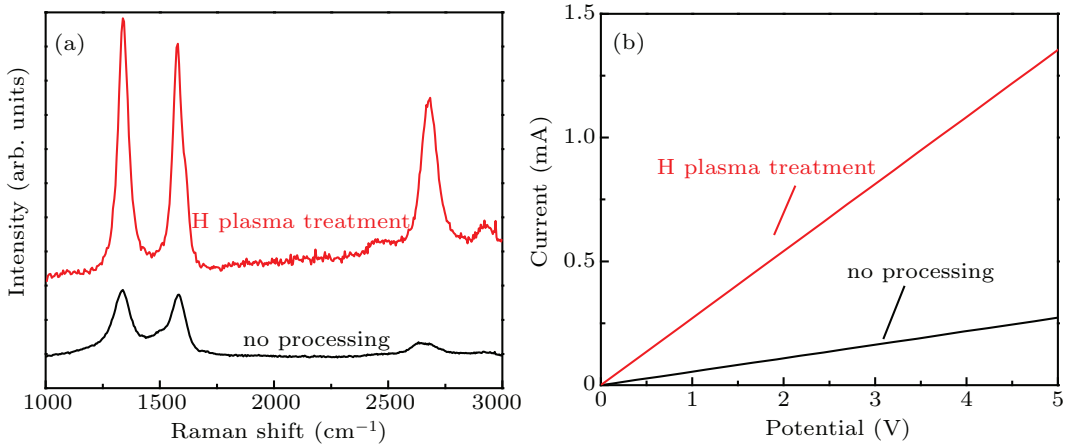


Fig. 3. (a) Raman spectra and (b) *I–V* curves of graphene-on-Willow glass samples before and after hydrogen plasma treatments.

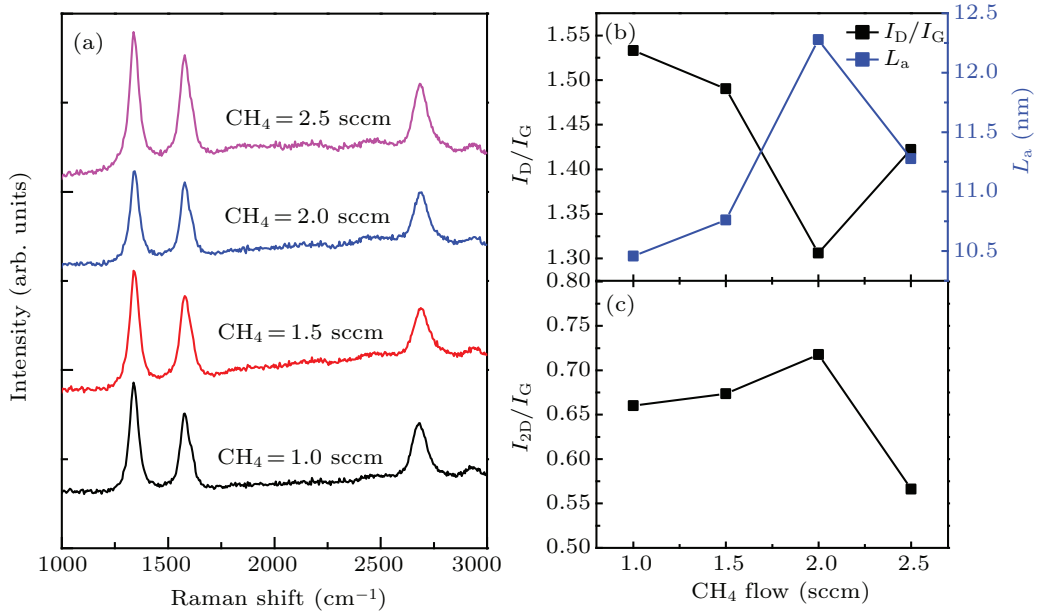


Fig. 4. (a) Raman spectra of graphene films prepared at different methane gas flow rates (1.0, 1.5, 2.0, and 2.5 sccm) grown on Willow glass; (b) I_D/I_G ratio (black curve) and grain size L_a (blue curve) varying with methane gas flow rate; (c) curve of I_{2D}/I_G varying with methane gas flow rate.

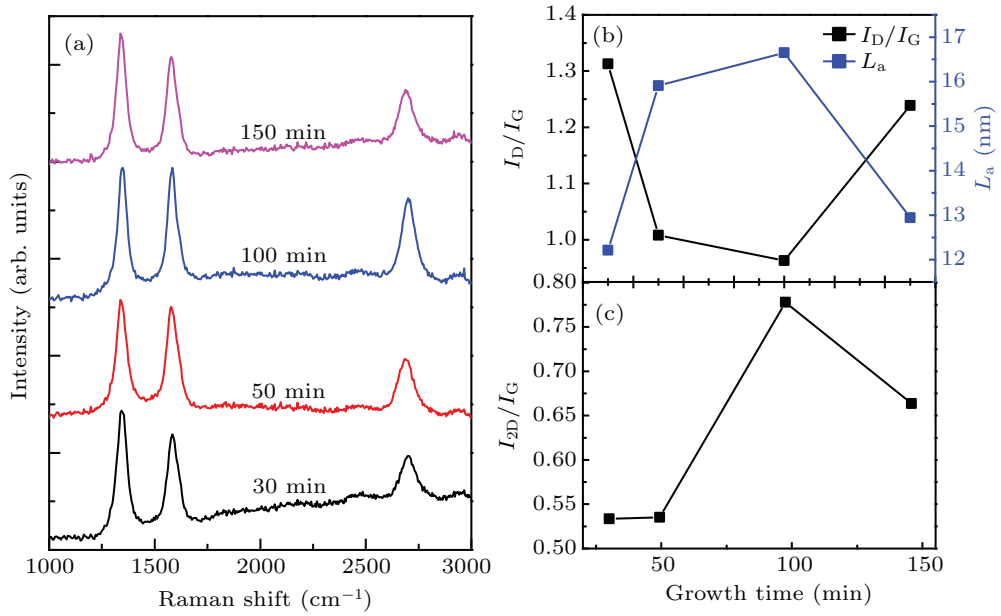


Fig. 5. (a) Raman spectra of graphene films on Willow glass, prepared at different growth times (30, 50, 100, and 150 min); (b) I_D/I_G ratio (black curve) and grain size L_a (blue curve) varying with growth time; (c) I_{2D}/I_G *versus* growth time.

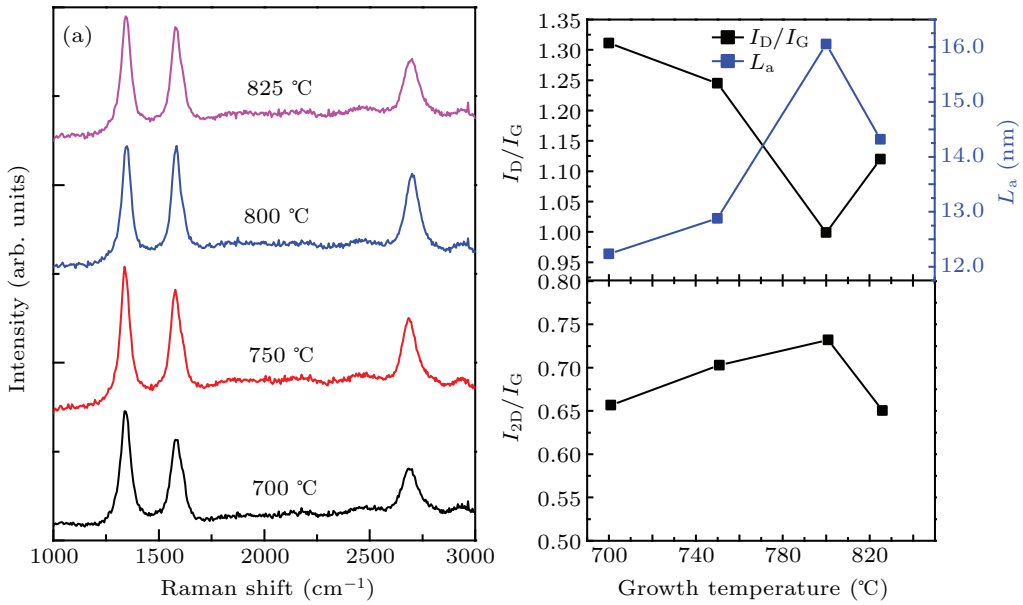


Fig. 6. (a) Raman spectra of the graphene films on Willow glass substrates grown at different temperatures (700, 750, 800, and 825 °C); (b) I_D/I_G ratio (black curve) and grain size L_a (blue curve) varying with growth time; (c) I_{2D}/I_G *versus* growth temperatures.

The effects of the growth temperature on the quality of graphene grown on willow glass are shown in Fig. 6. With growth temperature increasing from 700 °C to 825 °C, the I_D/I_G peak intensity ratio decreases. As the willow glass substrate melts at temperatures above 825 °C, 800 °C is identified as the optimal growth temperature for yielding the lowest I_D/I_G peak intensity ratio where the willow glass substrate is still stable. Therefore, 800 °C is used as the optimal growth temperature to improve the fraction of sp^2 C=C bonds and reduce the number of defects in the film.

As shown above, the optimized experimental parameters are a growth time of 100 min and mixed $CH_4/H_2/Ar$ gas flow rates of 2.0/8.0/200.0 sccm, respectively.

Figure 7 shows the macro and micro surface morphologies of the graphene films on the Willow glass substrates prepared at different values of RF powers ranging from 200 W to 300 W. Figure 7(a) shows the macroscopic morphology of the flexible Willow glass substrate (10 mm×10 mm) without and with the graphene film, revealing that all the films are homogeneous and have neither cracks nor holes. The transparency for each of the samples decreases with the augment of RF power, corresponding to an increase in the graphene film thickness. Higher RF power supports the completion of the cracking reaction of methane in the furnace, resulting in the obtainment of thicker graphene films on the substrates. Figures 7(b)–7(d) show the micrographs of the graphene films prepared at dif-

ferent values of RF power, revealing the microscopic surface morphologies. Figure 7(e) shows that a buffer layer is formed on the substrate surface in the initial stage, and that a small number of vertical graphene nanowalls appear on this buffer layer. With the increase of RF power, the nanowalls extend over the entire Willow glass surface due to the improved degree of gas ionization. The RF power determines the ionization degree of gas molecules in the furnace, which in turn affects the densities and activities of different species, such as high-energy electrons, ions, and atoms, in the reaction chamber. The buffer layer is a distinct 15-nm-thick layer between vertical graphene and the substrate and is composed of amorphous carbon and graphite as shown in Fig. 7(e).

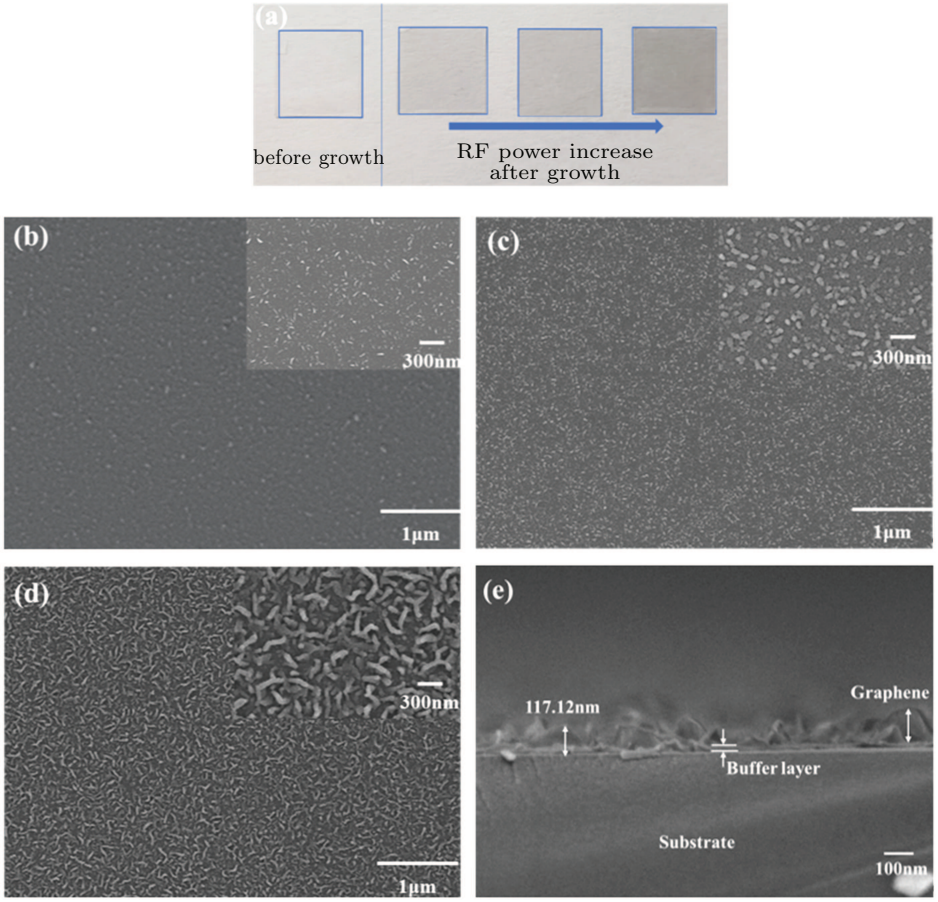


Fig. 7. (a) Macroscopic surface morphologies of graphene films, (b)–(d) micrographs of graphene/Willow glass substrates prepared at different values of RF power (b) 200, (c) 250, and (d) 300 W showing microscopic surface morphologies; (e) cross-sectional SEM image of graphene-Willow glass with RF power of 300 W.

Figures 8(a) and 8(b) show the XPS analysis of the graphene/Willow glass sample surfaces. Figure 8(a) shows the XPS survey spectrum, which contains the C 1s peak at 284.5 eV and O 1s peak at 531.4 eV. The atomic fractions of various elements are calculated from the XPS survey spectrum and found to be 95.23% and 4.77% for C 1s and O 1s, respectively. The existence of O1s peaks might be due to a small amount of oxygen adhering to the quartz tube wall and because of silicon hydride bond fracture as well. The high-resolution C 1s spectrum of graphene/Willow glass shown in Fig. 8(b) is deconvoluted into three components, including the sp^2 C=C peak at 284.5 eV (80.94 %), sp^3 C–C peak at 285.3 eV (15.28%), and C–O peak at 286.2 eV (3.78%).[34] The sharp peak is predominantly related to the sp^2 carbon bond,[35] which confirms that the synthesized material has a graphene structure.[36] Structure and morphology of the graphene/Willow glass are characterized by HR-TEM and from the corresponding selected-area electron diffraction (SAED) pattern. The HR-TEM image in Fig. 8(c) reveals that the graphene film has an interplanar spacing of 0.35 nm. The inset of Fig. 8(c) shows a clear diffraction ring pattern with spots, which indicates a polycrystalline structure due to interlaced grain boundaries, stitched grain patches in various orientations, or many layers.[37–39] The HRTEM image of the graphene/Willow glass in Fig. 8(d) shows that the prepared graphene films are composed of less than 10 layers of graphene. The corresponding 2D and three-dimensional (3D) AFM images confirm the vertically oriented morphologies of the graphene nanowalls grown on the flexible Willow glass.

The XRD is a common characterization method for the analysis of crystal structures of materials. Different diffraction peaks indicate the integrity and disorder of the spatial arrange-

ment of the graphene sheets, respectively. Figure 8(e) shows the x-ray diffraction pattern of the graphene/Willow glass sample, revealing a single sharp peak at 26.381°, which is assigned to the (002) plane. Based on the Bragg's law, the crystal plane spacing of the graphene film is obtained to be 0.338, which is consistent with the previously reported values.[40] A broad peak at around 10° may be attributed to the disordered graphene film.

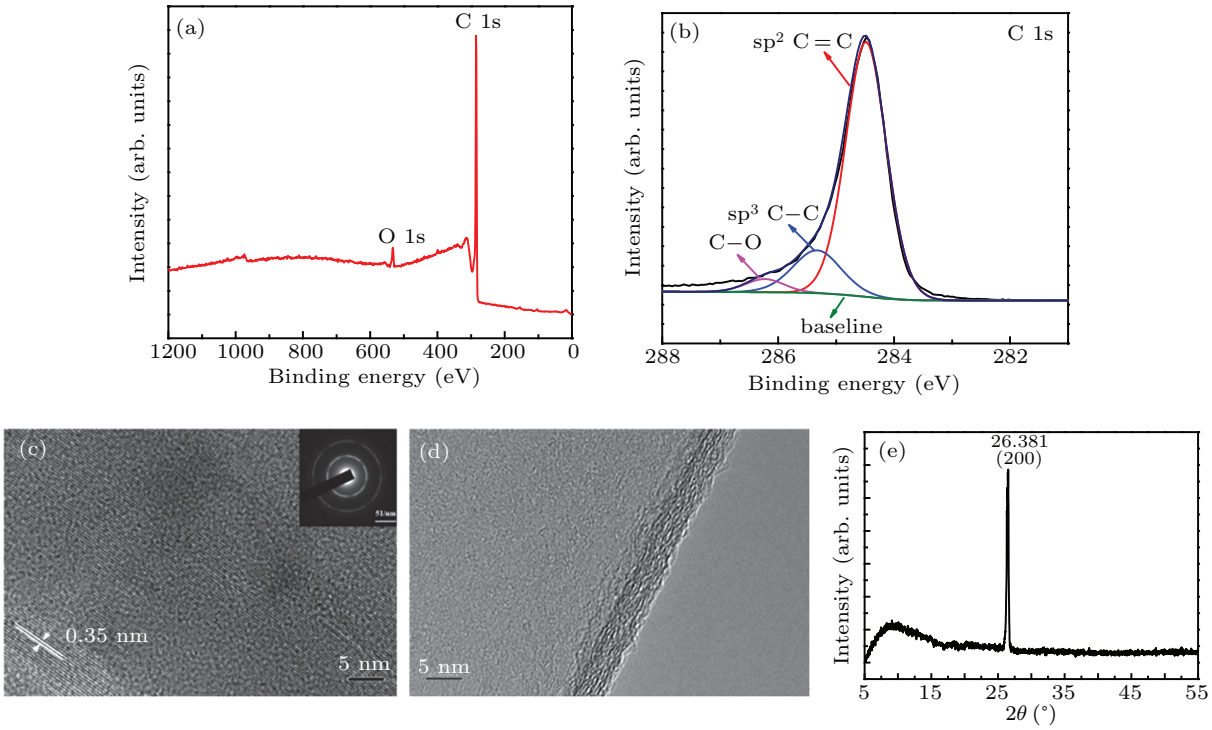


Fig. 8. (a) XPS survey spectrum, (b) C 1s high-resolution deconvolution peak spectra, (c) HR-TEM image and SAED pattern (inset image), (d) HR-TEM image (showing vertical graphene nanosheets), and (e) XRD pattern of graphene/Willow glass.

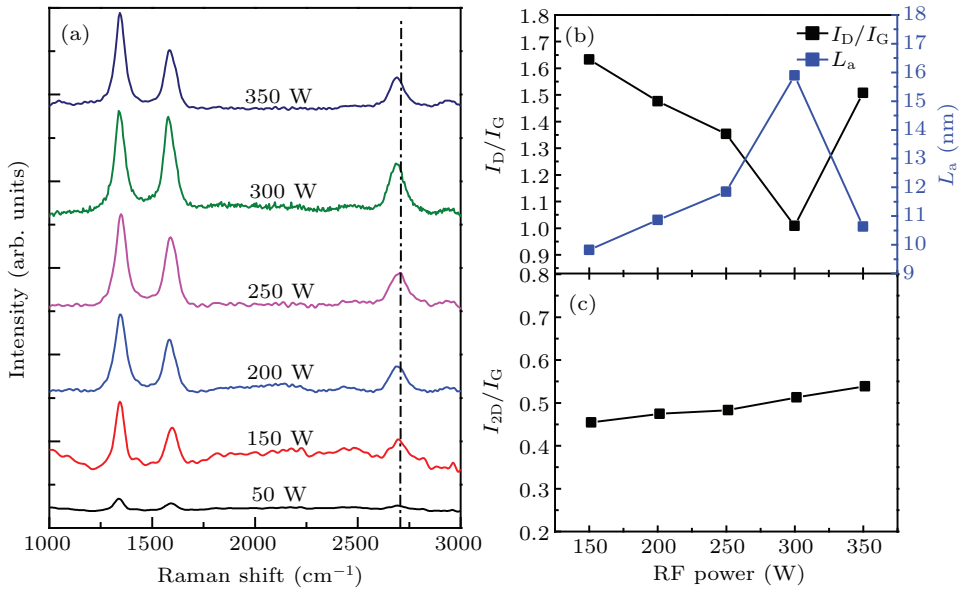


Fig. 9. (a) Raman spectra of the graphene films on Willow glass prepared at different values of RF powers (50, 100, 150, 200, 250, 300, and 350 W); (b) I_D/I_G ratio (black curve) and grain size L_a (blue curve) *versus* RF power; (c) I_{2D}/I_G ratio *versus* RF power.

Raman spectroscopy is one of the most prominent ways to determine the quality of graphene films.[18] Raman spectra of the graphene/Willow glass samples prepared at different values of RF power are shown in Fig. 9(a). When the RF power is 50 W, the D and G peaks are weak, and the 2D peak is negligible, indicating that only amorphous carbon clusters and graphite were deposited on the Willow glass surface. When the RF power increases from 50 W to 350 W, obvious 2D peaks appear. At low RF power, the formation of amorphous carbon film is favored in comparison with that of graphene films. With the increase of the RF power, the 2D peak position of graphene is blue-shifted slightly, which is attributed to the

decrease of the Fermi level velocity of the phonon dispersion and the change of the phonon dispersion curve caused by the superposition of multilayer graphene. The variation of I_D/I_G (black curve) and grain size L_a (blue curve) with RF power are shown in Fig. 9(b).

The grain size L_a has a negative correlation with the defect intensity ratio I_D/I_G. The I_D/I_G ratio decreases from 1.63 to 1.00 when the RF power increases from 150 W to 300 W, indicating the enhanced crystallinity of the graphene film. The I_D/I_G ratio can reach only about 1.00, which may be due to the edge gap between the upward graphene nanowalls. When the RF power is higher than 300 W, the I_D/I_G rises again. This may be due to the fact that when the RF power is too high, the carbon atoms are deposited too fast, and amorphous carbon atoms are agglomerated easily, resulting in a decrease in film quality. Figure 9(c) shows the variation of I_{2D}/I_G with the RF power. The I_{2D}/I_G ratio is around 0.5, indicating that the graphene nanowalls are composed of multiple layers, which is consistent with previous TEM analysis.

The optical and electrical properties of graphene/Willow glass are measured. Figure 10(a) shows the curves of light transmittance *versus* wavelength of the graphene samples at different values of RF power, which decrease with RF power increasing. The current–voltage (I–V) curves of graphene-Willow glass are shown in Fig. 10(b), indicating that the I–V slopes of the samples increase almost linearly when the RF power increasing from 50 W to 300 W. However, the slope decreases when the RF power is 350 W. This indicates that the conductivity of the graphene sample is improved as the RF power increase from 50 W to 300 W, while it decreases when the RF power is higher than 300 W, which is in agreement with the conclusion from previous analysis.

The electrical properties of graphene are investigated using a non-contact hall tester. The mobility of ordinary semiconductors is usually around 10^2 cm^2/(V·s)–10^6 cm^2/(V·s). Carriers in semiconductors are scattered mainly by defects and impurities at low temperatures. The carrier mobilities of the prepared graphene–Willow glass samples are much lower than those of monolayer graphene samples, which is probably due to the defects caused by discontinuities in the 3D graphene nanosheets and impurities generated during growth. According to the Hall effect, the Hall coefficients of p-type semiconductors are positive, and those of n-type semiconductors are negative. Therefore, the prepared graphene/Willow glass samples are identified as p-type doping. As shown in Table 1, the mobility decreases with carrier concentration increasing. The sheet resistance is less than 1 kΩ/sq, but it has a minimum value at 279.61 Ω/sq.

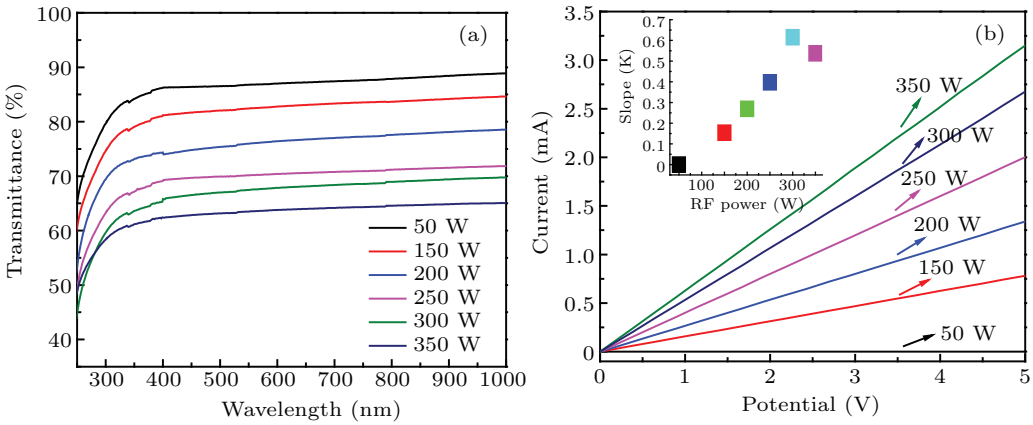


Fig. 10. (a) Variations of light transmittance with wavelength of the graphene/Willow glass sample prepared at different values of RF powers; (b) I–V curves of the graphene/Willow glass sample prepared at different RF powers.

Table 1. Photoelectric properties of graphene/Willow glass samples prepared at different values of RF power.

RF power (W)	Carrier mobility (cm^2·V^{-1}·s^{-1})	Carrier density (10^{14} cm^{-2})	Sheet resistance (Ω·sq^{-1})	Transmittance (550 nm)
150	37.41	3.699	529.65	86.80%
200	63.48	2.683	489.45	82.45%
250	131.27	1.404	359.94	70.14%
300	106.25	2.414	279.61	67.48%
350	125.36	2.045	304.35	63.52%

5. Conclusions

In summary, graphene films on a flexible Willow glass substrates are successfully prepared by a designed direct PECVD approach. The photoelectric properties and surface morphologies of the graphene–Willow glass can be adjusted by varying the growth parameters. In this paper, the influ-

ence of the RF power on the growth of graphene on flexible Willow glass is studied systematically, revealing that the RF power is an important parameter to modulate the photoelectric properties and surface morphology of graphene–Willow glass. The density and thickness of the graphene nanosheets on Willow glass increase significantly with the increase of the RF power. The 2D Raman peak intensity and the *I*–*V* slope of the graphene film increase as the RF power increases from 50 W to 300 W. The light transmittance increases with the augment of the RF power. However, when the RF power exceeds 300 W, the properties of the graphene–Willow glass degrade. The non-catalytic direct synthesis of graphene is one of the keys to the industrial production of flexible graphene devices. Therefore, our research is of great significance in developing transparent flexible electronics.

References

[1] Geim A K and Novoselov K S 2007 *Nat. Mater.* **6** 183
[2] Su C Y, Lu A Y, Xu Y, Chen F R, Khlobystov A N and Li L J 2011 *Acs Nano* **5** 2332
[3] Hernandez Y, Nicolosi V, Lotya M, Blighe F M, Sun Z, De S, McGovern I T, Holland B, Byrne M, Gun'ko Y K, Boland J J, Niraj P, Duesberg G, Krishnamurthy S, Goodhue R, Hutchison J, Scardaci V, Ferrari A C and Coleman J N 2008 *Nat. Nanotechnol.* **3** 563
[4] Liu Q B, Yu C, Li J, Song X B, He Z Z, Lu W L, Gu G D, Wang Y G and Feng Z H 2014 *Chin. Phys. Lett.* **31** 078104
[5] Ismach A, Druzgalski C, Penwell S, Schwartzberg A, Zheng M, Javey A, Bokor J and Zhang Y 2010 *Nano Lett.* **10** 1542
[6] Teng P Y, Lu C C, Akiyama-Hasegawa K, Lin Y C, Yeh C H, Suenaga K and Chiu P W 2012 *Nano Lett.* **12** 1379
[7] Hao Y, Bharathi M S, Wang L, Liu Y, Chen H, Nie S, Wang X, Chou H, Tan C, Fallahazad B, Ramanarayan H, Magnuson C W, Tutuc E, Yakobson B I, McCarty K F, Zhang Y W, Kim P, Hone J, Colombo L and Ruoff R S 2013 *Science* **342** 720
[8] Li D, Mueller M B, Gilje S, Kaner R B and Wallace G G 2008 *Nat. Nanotechnol.* **3** 101
[9] Tung V C, Allen M J, Yang Y and Kaner R B 2009 *Nat. Nanotechnol.* **4** 25
[10] Al-khattib M G, Samir A and Hassaballa S 2020 *Opt. Quantum Electron.* **52** 217
[11] Dai B, Fu L, Zou Z, Wang M, Xu H, Wang S and Liu Z 2011 *Nat. Commun.* **2** 522
[12] Luo W G, Wang H F, Cai K M, Han W P, Tan P H, Hu P A and Wang K Y 2014 *Chin. Phys. Lett.* **31** 607207
[13] Rybin M G, Kondrashov, II, Pozharov A S, Nguyen V C, Phan N M and Obraztsova E D 2018 *Phys. Status Solidi B* **255** 1700414
[14] Losurdo M, Giangregorio M M, Capezzuto P and Bruno G 2011 *Phys. Chem. Chem. Phys.* **13** 20836
[15] Zhang Y, Fu Y, Edwards M, Jeppson K, Ye L and Liu J 2017 *Mater. Lett.* **193** 255
[16] Chugh S, Mehta R, Lu N, Dios F D, Kim M J and Chen Z 2015 *Carbon* **93** 393
[17] Sun J, Chen Y, Cai X, Ma B, Chen Z, Priydarshi M K, Chen K, Gao T, Song X, Ji Q, Guo X, Zou D, Zhang Y and Liu Z 2015 *Nano Res.* **8** 3496
[18] Mischke J, Pennings J, Weisenseel E, Kerger P, Rohwerder M, Mertin W and Bacher G 2020 *2D Mater.* **7** 035019
[19] Pham V P, Jang H S, Whang D and Choi J Y 2017 *Chem. Soc. Rev.* **46** 6276
[20] Marchena M, Janner D, Chen T L, Finazzi V and Pruneri V 2016 *Opt. Mater. Express* **6** 2487
[21] Wei N, Li Q, Cong S, Ci H, Song Y, Yang Q, Lu C, Li C, Zou G, Sun J, Zhang Y and Liu Z 2019 *J. Mater. Chem. A* **7** 4813
[22] Shan J, Cui L, Zhou F, Wang R, Cui K, Zhang Y and Liu Z 2020 *Acs Appl. Mater. Interfaces* **12** 11972
[23] Yang C Y, Bi H, Wan D Y, Huang F Q, Xie X M and Jiang M H 2013 *J. Mater. Chem. A* **1** 770
[24] Ci H, Ren H, Qi Y, Chen X, Chen Z, Zhang J, Zhang Y and Liu Z 2018 *Nano Res.* **11** 3106
[25] Zhang L F, Feng S P, Xiao S Q, Shen G, Zhang X M, Nan H Y, Gu X F and Ostrikov K 2018 *Appl. Surf. Sci.* **441** 639
[26] Yang X, Tang S, Ding G, Xie X, Jiang M and Huang F 2012 *Nanotechnology* **23** 025704
[27] Zhang W, Wu P, Li Z and Yang J 2011 *J. Phys. Chem. C* **115** 17782
[28] Chu J, Han Y J, Li Y M, Jia P F, Cui H, Duan S K, Feng P T and Peng X Y 2020 *J. Phys. D: Appl. Phys.* **53** 3251019
[29] Mohanta A, Lanfant B, Asfaha M and Leparoux M 2017 *Appl. Phys. Lett.* **110** 093109
[30] Chang Y C, Yen C C, Tsai H C, Chen T C, Yang C M, Chen C H and Woon W Y 2020 *Carbon* **159** 570
[31] Ivan Vlassiouk M R, Pasquale Fulvio, Sheng Dai, Panos Datskos, Gyula Eres and Sergei Smirnov 2011 *Carbon* **5** 6069
[32] Wang H, Zhou Y, Qi M, Liu C, Xu X and Ren Z 2018 *J. Phys. Chem. C* **123** 2370
[33] Tuinstra F and Koenig J L 1970 *J. Chem. Phys.* **53** 1126
[34] Zhao G, Shao D, Chen C and Wang X 2011 *Appl. Phys. Lett.* **98** 183114
[35] Yang D, Velamakanni A, Bozoklu G, Park S, Stoller M, Piner R D, Stankovich S, Jung I, Field D A, Ventrice C A and Ruoff R S 2009 *Carbon* **47** 145
[36] Basumatary B, Podder S, Sharma B, Pal A R, Sahariah M B, Sen Sarma N and Patil D S 2020 *J. Electron. Mater.* **49** 5467
[37] Zhao M, Xue Z, Zhu W, Wang G, Tang S, Liu Z, Guo Q, Chen D, Chu P K, Ding G and Di Z 2020 *Acs Appl. Mater. Interfaces* **12** 15606
[38] Li J R, Liu Z D, Guo Q L, Yang S W, Xu A L, Wang Z W, Wang G, Wang Y Q, Chen D and Ding G Q 2019 *J. Mater. Chem. C* **7** 5995
[39] Gunes F, Han G H, Kim E S, Chae S J, Park M H, Jeong H K, Seong Chu Lim and Young Hee Lee 2009 *Nano* **4** 83
[40] Wang L, Wang Y, Xu T, Liao H, Yao C, Liu Y, Li Z, Chen Z, Pan D, Sun L and Wu M 2014 *Nat. Commun.* **5** 5357